ORIGINAL SCIENTIFIC PAPER

CROATICA CHEMICA ACTA

Croat. Chem. Acta **2025**, *98*(1), 53–63
Published online: May 16, 2025
DOI: 10.5562/cca4153

HKD 1926

A Computational Study of the Chemical Reactivity of the (2S,3R) and (2S,3S) Isomers of Dehydrated Hydroxycitric Acid

Wendolyne López-Orozco, Luis Humberto Mendoza-Huizar,* Giaan Arturo Álvarez-Romero, Maricruz Sánchez-Zavala

Área Académica de Química, Universidad Autónoma del Estado de Hidalgo, carretera Pachuca–Tulancingo, 42183, Mineral de la Reforma, Hidalgo. México
* Corresponding author's e-mail address: hhuizar@uaeh.edu.mx

RECEIVED: November 25, 2024 ✶ REVISED: March 11, 2025 ✶ ACCEPTED: March 15, 2025

Abstract: A computational investigation about the chemical reactivity of hibiscus acid (HA) and garcinia acid (GA) diastereoisomers was conducted using the X/6-311G(d,p) theoretical level (where X = B3LYP, B3PW91, BHandHLYP and WB97XD). Analysis of global reactivity descriptors revealed similar behavior for both diastereoisomers. However, Fukui function calculations highlighted differences in local active site distribution attributed to the orientation of the hydroxyl group at C3 in the oxolane structure. Variations in carboxyl group orientations were observed to induce distinct local reactivities on the HA and GA due to the presence of different intramolecular interactions, which are impacting their chemical properties. Also, specific sites susceptible to nucleophilic, electrophilic, and free radical attacks were identified. NBO results were used to estimate the donor-acceptor interactions in HA and GA. The results suggest that the most favorable interactions are LP(2)O17 and BD*(2) C9-O19. Additionally, an analysis of the bond critical points (BCPs) indicates that the Laplacian of the density in GA is higher compared to HA, suggesting that the BCP in GA is more sensitive to variations in the surrounding electronic density. These findings could provide an explanation for the observed differences in reactivity between these compounds.

Keywords: Hibiscus acid, Garcinia acid, chemical reactivity, diastereoisomers, non covalent interactions, NBO, AIM.

INTRODUCTION

OBESITY, characterized by excessive accumulation of body fat, emerges as the primary risk factor driving the onset and progression of type 2 diabetes mellitus (DM) across all age groups. Its prevalence has reached alarming levels akin to a pandemic, emphasizing the urgent need for comprehensive strategies addressing both obesity and diabetes management to curb its impact. In the case of obesity, lifestyle modifications like dietary changes and exercise are fundamental for long-term prevention, but they often fall short of achieving significant or sustainable weight loss. Consequently, the demand for treatment options becomes imperative.[1–3] Hence, obesity can be addressed with medications such as phentermine, sibutramine, orlistat, and rimonabant, all of which are licensed for weight reduction therapy.[4,5] However, it is essential to note that these medications may induce side effects like dry mouth, insomnia, and fatigue. Moreover, drugs like sibutramine have been withdrawn from the market due to severe cardiovascular risks.[4] On the other hand, in the treatment of patients with diabetes who require medication for obesity, healthcare providers often utilize GLP-1 agonists such as semaglutide, dulaglutide, and liraglutide,[6] or SGLT2 inhibitors like empagliflozin, dapagliflozin, canagliflozin, ertugliflozin,[7] among others. The most common side effects of GLP-1 agonists include loss of appetite, nausea, vomiting, abdominal pain, diarrhea, dizziness, mild tachycardia, infections, headaches, and indigestion (upset stomach).[8] On the other hand, the primary adverse events associated with SGLT2 inhibitors include urinary tract and genital infections, as well as euglycemic diabetic ketoacidosis.[9] Thus, it is necessary to search for less aggressive treatments, among which natural products and plant-based supplements, which have been utilized for centuries, are gaining recognition for their effectiveness in treating diseases and maintaining health.[4]

Hydroxycitric acid (1,2-dihydroxypropane-1,2,3-tricarboxylic acid) is a phytomolecule derivative of citric acid that naturally occurs in a variety of plants, including Garcinia cambogia,[10–13] and Hibiscus subdariffa.[14–16] Hydroxycitric acid (HCA) is widely utilized in medicines and as food additives,[17] and has been found to be a potential metabolic regulator with antiobesity activity,[18,19] an inhibitor of lipogenesis,[19–23] and hypoglycemic.[24] HCA has two diastereomers due to the presence of two chiral centers in the molecule. Consequently, there are four stereoisomers of HCA, consisting of two pairs of enantiomers, thus, HCA exists in four different isomers. However, only the (2S,3R)-tetrahydro-3-hydroxy-5-oxo-2,3-furandicarboxylic acid, [(2S,3R)-2] known as hibiscus acid, see Figure 1a, and its diastereomer, (2S,3S)-tetrahydro-3-hydroxy-5-oxo-2,3-furandicarboxylic acid [(2S,3S)-2] referred to as garcinia acid, see Figure 1b, have been reported as bioactive compounds for antidiabetic,[25] and antiobesity effects,[18] respectively. In this context, the (2S, 3S) isomer inhibits ATP citrate lyase, while the (2S, 3R) isomer acts on pancreatic alpha-amylase and alpha-glucosidase enzymes.[18,21] Although it is well known that hibiscus acid and garcinia acid are organic compounds containing acidic groups, and their reactivity may be of interest in various areas such as medicinal chemistry and nutrition, most studies have focused on their therapeutic activity and physiological properties.[5,14,26–31] Although, recently, a theoretical study was conducted to identify the reactivity of hydroxycitric acid in its open-chain form using global and local reactivity descriptors derived from DFT theory;[32] it has been reported that isolating stereoisomers of HCA in their open-chain forms is exceedingly challenging. Moreover, due to the γ-hydroxyl group's tendency to spontaneously undergo lactonization, it forms a γ-butyrolactone ring system during isolation.[33] Thus, a study of the molecular reactivity of HCA in its lactone forms, which are available naturally, is still missing. However, to the best of our knowledge, after a search in the literature, no molecular-level study has been conducted to study the chemical reactivity at the molecular level of the stereoisomers of hydroxycitric acid lactones in their configurations (2S, 3S) and (2S, 3R). Therefore, investigating their reactivity could yield valuable insights into how these compounds interact with other chemical and biological systems. Furthermore, this kind of studies may offer insights into potential reaction mechanisms and aid in optimizing the synthesis of these compounds. Thus, in this work, we conducted a computational study of the chemical reactivity of hydrocyclic acid in its (2S, 3S) and (2S, 3R) configurations to enhance the understanding that exists on this subject.

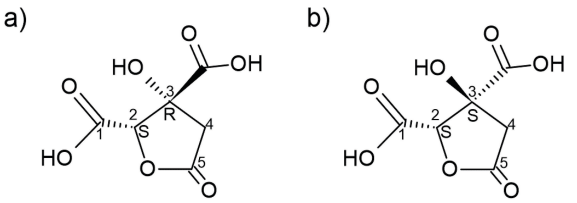

Figure 1. Chemical structure of hibiscus acid ((2*S*,3*R*)-3-hydroxy-5-oxooxolane-2,3-dicarboxylic acid) and garcinia acid ((2*S*,3*S*)-3-hydroxy-5-oxooxolane-2,3-dicarboxylic acid).

THEORY

Global Reactivity Parameters

Chemical reactivity of HA and GA was evaluated through global and local chemical reactivity descriptors derived from the density functional theory.[34,35] The global descriptors used are the electronic chemical potential (μ), the hardness (η) value, and the electronegativity (χ). μ allows us to measure the electron escape tendency from the molecule, χ is the negative of the electronic chemical potential, and η allows us to analyze the molecular stability. These descriptors may be evaluated through the [Eq. (1–3)]:[34,35]

$$\mu = \left(\frac{\partial E}{\partial N}\right)_{v(r)} = -\frac{1}{2}(I + A) = \frac{1}{2}(\varepsilon_L + \varepsilon_H) \quad (1)$$

$$\chi = -\mu \quad (2)$$

$$\eta = \left(\frac{\partial \mu}{\partial N}\right)_{v(r)} = \left(\frac{\partial^2 \mu}{\partial N^2}\right)_{v(r)} = (I - A) = (\varepsilon_L - \varepsilon_H) \quad (3)$$

In these equations, I is the ionization potential, A is the electronic affinity, ε_L is the energy of the lowest unoccupied molecular orbital (LUMO), and ε_H is the energy of the highest occupied molecular orbital (HOMO). Also, the electrophilicity index was determined to identify the nucleophile or electrophile character of the molecular system as:[36]

$$\omega = \frac{\mu^2}{2\eta} \quad (4)$$

while the electroacceptation power (ω^-) or electrodonation charge power (ω^+) were evaluated by:

$$\omega^- = \frac{(\mu^-)^2}{2\eta} = \omega^- = \frac{\left(-\frac{1}{4}(3I + A)\right)^2}{2(I - A)} = \frac{\left(-\frac{1}{4}(3\varepsilon_L + \varepsilon_H)\right)^2}{2(\varepsilon_L - \varepsilon_H)} \quad (5)$$

$$\omega^+ = \frac{(\mu^+)^2}{2\eta} = \omega^- = \frac{\left(-\frac{1}{4}(I + 3A)\right)^2}{2(I - A)} = \frac{\left(-\frac{1}{4}(\varepsilon_L + 3\varepsilon_H)\right)^2}{2(\varepsilon_L - \varepsilon_H)} \quad (6)$$

Local Reactivity Parameters

In order to identify the regions more susceptible to receiving nucleophilic, electrophilic, or free radical attacks, we evaluated the Fukui function (FF) as the variation of electron density $p(r)$ with a fixed geometry and the external potential constant ($v(r)$) as the number of electrons change (N), [Eq. (7)]:

$$f(r) = \left(\frac{\partial \rho(r)}{\partial N} \right)_{v(r)} = \left(\frac{\partial \mu(r)}{\partial (r)} \right) \quad (7)$$

FF was evaluated following three different approximations, which are: a) frozen-core (FC), b) finite difference (FD),[37] and c) atomic charges.[38] The equations for each approximation are reported in the supplementary material to evaluate FF for nucleophilic ($f^+(r)$), electrophilic ($f^-(r)$) and free radical attacks ($f^0(r)$).

METHODS

The HA and GA structures were subjected to full geometrical optimization in the aqueous phase employing the X/6-311G (d,p) level of theory,[39] (where X = B3LYP,[40,41] B3PW91,[42] BHandHLYP,[43] and WB97XD[44]). The solvent phase was taken into account employing the continuous polarizable model (PCM) developed by Tomasi et al.[45,46] Vibrational frequencies were calculated to ensure that the stationary points corresponded to a minimum on the potential energy surface. All quantum calculations reported here were performed with the package Gaussian 09,[47] and visualized with the packages GaussView,[48] Arguslab,[49] Gabedit,[50] and Multwfn.[51] NBO calculations,[52] were performed as implemented in the package Gaussian 09.[47]

RESULTS AND DISCUSSION

Geometry Optimization

The molecular structures of HA and GA were optimized, without restrictions, at the X/6-311G (d,p) level of theory,[39] (where X = B3LYP,[40,41] B3PW91,[42] BHandHLYP,[43] and WB97XD[44]), similar results were obtained using the different functionals employed in the calculations, and the optimized structures are depicted in Figure 2. In the case of HA, the C-C, C=O and O-H distances, and angles, and dihedral angles are very close to those obtained from X-ray crystallography.[53] Also, the vibrational frequencies for the optimized HA and GA structures were calculated at the theoretical level X/6-311G (d,p),[39] and all of them are real (positive numbers), confirming that the geometry is genuinely a minimum on the X/6-311G (d,p) potential energy surface. The vibrational frequencies evaluated at the B3LYP/6-311G (d,p) level of theory have been uniformly adjusted by a factor of 0.9888.[54] HA and GA displayed strong IR bands at 3706, 1816, 1354, and 1148 cm^{-1} (see Figure 1S in the supplementary material), which correspond to O-H stretching, C=O stretching, C-C stretching and C-C bending in the plane, respectively. These values are close to those reported in the literature for HA,[53] and GA.[20]

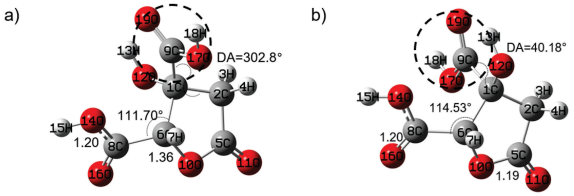

Figure 2. Optimized structures of a) HA, and b) GA at the B3LYP/6-311G (d,p) level of theory in the aqueous phase employing the PCM solvation model. Bond distances are given in Angstroms, DA=Dihedral Angle.

Global Reactivity Descriptors

The chemical reactivities of HA and GA were analyzed through the global reactivity descriptors given by [Eq. (1–6)] and are reported in Table 1 and 2, respectively. Note that the hardness values are very similar for both diasteroisomers, indicating that the orientation of the carboxyl substituent does not have a significant effect on global chemical stability. Similar tendencies were observed with the values of μ, χ, ω for both diasteroisomers, suggesting the same global chemical behavior for these compounds.

Table 1. Global reactivity descriptors calculated for HA evaluated at the X/6-311G (d,p) level of theory,[39] (where X = B3LYP,[40,41] B3PW91,[42] BHandHLYP,[43] and WB97XD[44]) and in the aqueous phase, using [Eq. (1–6)]. The values in parentheses correspond to the values calculated using Koopman's theorem.

	μ / eV	η / eV	χ / eV	ω / eV	ω^+ / eV	ω^- / eV
B3LYP	4.48 (4.51)	7.01 (7.13)	–4.48 (–4.51)	2.86 (2.85)	2.77 (2.78)	0.53 (0.52)
B3PW91	4.49 (4.52)	7.02 (7.12)	–4.49 (–4.52)	2.87 (2.87)	2.77 (2.79)	0.53 (0.53)
BHandHLYP	4.56 (4.36)	10.53 (7.87)	–4.56 (4.36)	1.98 (2.41)	0.18 (2.54)	2.46 (0.36)
WB97XD	4.78 (4.78)	11.30 (7.57)	–4.78 (–4.78)	1.01 (1.51)	0.17 (0.55)	2.56 (2.94)

Table 2. Global reactivity descriptors calculated for GA evaluated at the X/6-311G (d,p) level of theory,[39] (where X = B3LYP,[40,41] B3PW91,[42] BHandHLYP,[43] and WB97XD[44]) and in the aqueous phase, using [Eq. (1–6)]. The values in parentheses correspond to the values calculated using Koopman's theorem.

	μ / eV	η / eV	χ / eV	ω / eV	ω^+ / eV	ω^- / eV
B3LYP	4.37 (–4.39)	6.99 (–7.09)	–4.37 (–4.39)	2.73 (–2.72)	2.67 (–2.68)	0.49 (–0.48)
B3PW91	4.49 (–4.4)	7.02 (–7.07)	–4.49 (–4.4)	2.87 (–2.74)	2.77 (–2.69)	0.53 (–0.49)
BHandHLYP	4.56 (–4.45)	10.53 (–8.32)	–4.56 (–4.45)	1.98 (–2.38)	0.18 (–2.56)	2.46 (–0.34)
WB97XD	4.65 (–4.71)	11.29 (–7.66)	–4.65 (–4.71)	0.96 (–1.45)	0.15 (–0.51)	2.47 (–2.87)

Local Reactivity Descriptors

The distribution of the more reactive sites in a molecular system can be evaluated through the Fukui Function (FF) by using the FC (equations 1S and 2S) and FD (equations 3S-5S) approximations; see equations in the supplementary material. In the case of the FC approach, the more reactive sites to electrophilic attacks are given by the sites with a higher contribution from the HOMO orbital (Fig. 3a and 3b), while the nucleophilic sites are given by the sites with a higher contribution from the LUMO orbital (Fig. 3c and 3d). Note that the distribution of the frontier orbitals varies depending on the carboxyl chiral substituent orientation. Also, observe that the major contribution of the HOMO orbital in the HA molecule (Fig. 3a) is on the oxygen atom in the oxolane carbonyl group, followed by the oxygen atom in the hydroxyl group located at C-3, and in the carbon atoms at C-3 and C-4. For GA (Fig 3b), the major contributions of HOMO's orbital are observed on the oxygen atom in the oxolane carbonyl group and on the oxygen atom of the hydroxyl group at C-3, followed by the C-3, C-4, and C-5 carbon atoms. Also, it is possible to observe that the carbon and oxygen atoms in the carbonyl group at C-2 show the lowest HOMO contribution in GA. If one analyzes the LUMO distribution on HA and GA, it is possible to identify the more reactive sites for nucleopilic attacks. For the HA molecule (Fig. 3c), the highest LUMO contribution is on the carbon atom in the carbonyl group at C-3, followed by the oxygen atoms in the carbonyl group at C-3, and on the C-1 carbon atom. The lowest contribution is found on the oxygen atoms in the carboxyl group at C-2. In the case of GA (Fig. 3d), the higher contribution of LUMO orbitals is located on the carbon atom in the carbonyl group at C-2, while a lower distribution was observed on the oxygen atoms in the carbonyl group at C-3 and on the carbon and oxygen atoms in the oxolane carbonyl. In summary, the results suggest that the orientation of the carbonyl group in HA and GA is causing the more reactive sites for electrophilic attacks to be on the carbonyl at C-3 in HA, while for GA, it is on the carbonyl group at C-2. For nucleophilic attacks, the more reactive site is on the carbonyl group at C-2 in HA and in the oxolane carbonyl group for GA.

The evaluation of the Fukui Function using the FD approximation (equations (3S)-(5S) in the supplemental material) is reported for HA (Figure 4) and GA (Fig. 5). The more susceptible sites to nucleophilic attacks in HA were located on the carboxyl at the C-3, due to the positive polarity on the carbon atom (Fig. 4a). For electrophilic attacks, the more active sites were the oxygen atom of the carbonyl group in the carboxyl of the C-3 in the oxygen atom in the oxolane carbonyl and the hydroxyl group at the C-3, due to their electronic abundance (Fig. 4b). For free radical attacks, the more reactive sites are found on the carboxyl groups and in the oxygen in the oxolane (Fig. 4c). For GA molecules, the more susceptible sites to nucleophilic attack are found on the carboxyl group at C-3 and on the oxygen atom in the oxolane group (Fig. 5a). In the case

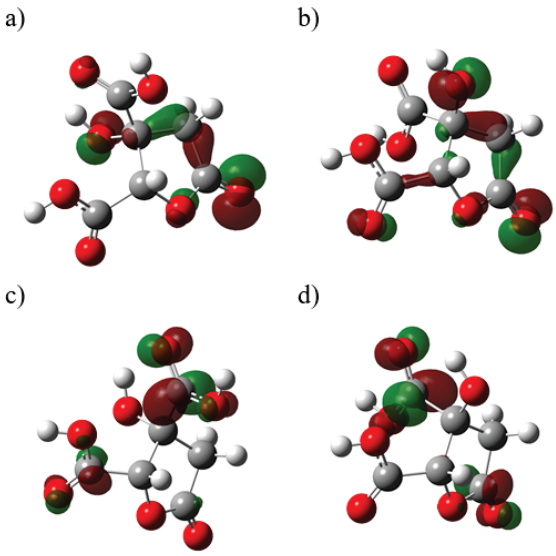

Figure 3. HOMO distributions for a) hibiscus acid and b) garcinia acid, and LUMO distributions for c) hibiscus acid and d) garcinia acid were obtained at the WB97XD/6-311G(d,p) level of theory in the aqueous phase using the PCM solution model. In all cases, the isosurfaces were obtained at 0.02 e/a.u.^{3}.

of electrophilic attacks, the more reactive positions are found on the oxygen atom of the carbonyl group in the carboxyl at C-2, in the oxygen atom in the oxolane group, and in the hydroxyl group at C-3 (Fig. 5b). In the case of free radical attacks, the more reactive zones of the molecule are located on the carboxyl at C-2 and C-3 and in the oxygen atom in the oxolane (Fig. 5c). The above mentioned indicates that when the hydroxyl substituent is pointing back in the oxolane structure in the case of GA, the carboxyl substituent at C-3 attracts electron density, and therefore the oxolane carbonyl becomes susceptible to a nucleophilic attack. In comparison with HA the only site susceptible to a nucleophilic attack is on the carboxyl at C-3.

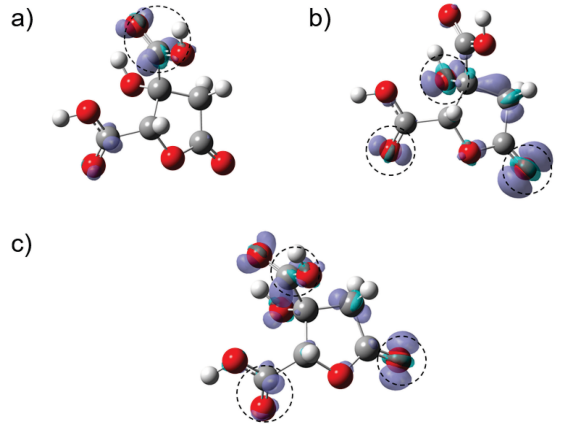

Figure 4. Isosurfaces of the Fukui Functions for HA according to equations (3S), (4S), and (5S), in the supplemental material at the WB97XD/6-311G(d,p) level of theory employing the PCM solvation model. In the case of (a) nucleophilic, (b) electrophilic, and (c) free radical attacks. In all cases, the density isosurfaces were obtained at 0.01 e/a.u.^{3}, dashed circles show the more reactive zones in each molecule.

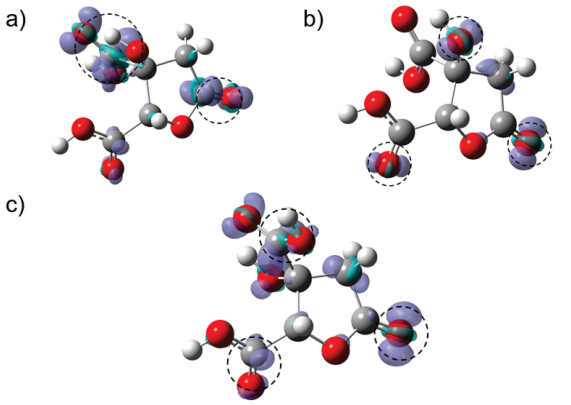

Figure 5. Isosurfaces of the Fukui functions for GA according to equations (3S), (4S), and (5S), in the supplemental material, at the WB97XD/6-311G(d,p) level of theory employing the PCM solvation model. In the case of (a) nucleophilic, (b) electrophilic, and (c) free radical attacks. In all cases, the isosurfaces were obtained at 0.01 e/a.u.^{3}, dashed circles show the more reactive zones in each molecule.

Also, it is possible to condense the Fukui function through equations (6S), (7S), and (8S) to identify the pinpoint distribution of active sites because the highest CFF values correspond to the more reactive atoms in the reference molecule.[55] In the case of equations (6S)-(8S), we used the Hirshfeld population to evaluate the CFF values because the values obtained are non-negative.[56,57] The CFF values for nucleophilic attacks at different levels of theory for the molecules in the aqueous phase are reported in Table 3 for HA and in Table 4 for GA. Note that HA exhibits the more susceptible site for nucleophilic attacks on the carboxyl at C-3 and the more susceptible sites to electrophilic attack are on the oxygen atom of the carbonyl group of the carboxyl at C-2 and the oxygen in the oxolane carbonyl. In the case of free radical attacks, the more reactive sites are on the oxygen in the oxolane and on the carbonyl group at C-3. While for GA, see Table 4, the more reactive zone towards nucleophilic attack is the carboxyl located at C-3 and also on the oxygen in the oxolane. On

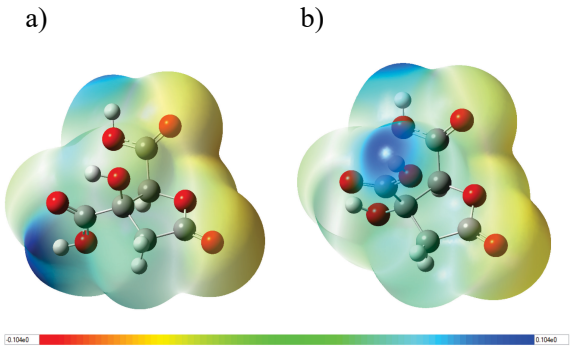

Figure 6. Mapping of the electrostatic potentials evaluated at the WB97XD /6-311G (d,p) level of theory using the PCM solvation model on a density isosurface (p =0.002 e/a.u.^{3}) for a) HA and b) GA.

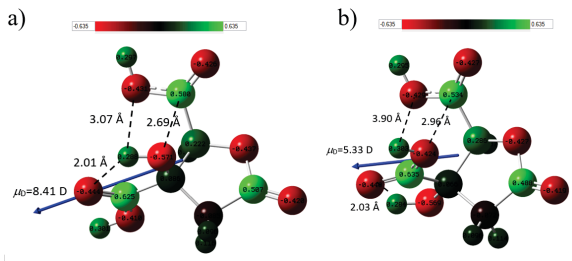

Figure 7. Mulliken population analysis for a) HA and b) GA.

the other hand, in the case of the more reactive sites for electrophilic and free radical attacks, GA had the same behavior as HA. Similar results were obtained at the four levels of theory employed in this work.

Also, it is possible to analyze the chemical reactivity of molecules through molecular electrostatic potential maps (MEP).[31] Figure 6 shows the MEP of HA and GA. In this figure, the negative potential areas (red color) represent electron-abundant zones, while the positive potential areas (blue color) show a relative lack of electrons. The results indicate that the carboxyl and hydroxyl groups at C-2 and C-3 of GA exhibit more negative potential values in comparison to the hydroxyl groups at C-2 and C-3 of HA, suggesting that the substituents of the (2*S*,3*S*) conformation are more electrophilic compared to the substituents of the (2*S*,3*R*) conformation. Additionally, the charge distribution for HA and GA was analyzed, as shown in Figure 7. The different charge distributions in both molecules result in dipole moment values of 8.41 D (HA, Figure 7a) and 5.31 D (GA, Figure 7b), indicating a variation in the charge distribution within the molecules. Since the dipole moment is a measure of charge separation, a value of 8.41 D suggests a more uneven or polarized charge distribution compared to the value of 5.31 D. This difference could influence non-covalent interactions. The figure shows that this charge distribution is related to the separation between the -COOH and the OH groups.

Analysis Of Non-Covalent Interactions

The chemical reactivity study revealed that both diasterosiomers show similar global reactivity but different local reactivity due to the different orientations of the carboxyl substituents. In order to identify the interactions involved in both diasteroisomers and if these interactions are significant, it was analyzed the regions where the reduced gradient will have values close to zero to identify regions of covalent bonding and non-covalent interactions through the NCI index, equation (8).[54]

$$s(r) = \frac{1}{2(2\pi^2)^{1/3}} \frac{|\nabla\rho(r)|}{\rho(r)^{4/3}} \quad (8)$$

Table 3. Condensed Fukui function values for nucleophilic attacks on HA at the X/6-311G (d,p) level of theory,[39] (where X = B3LYP,[40,41] B3PW91,[42] BHandHLYP,[43] and WB97XD[44]), in the aqueous phase employing Hirshfeld population and equations (6S-8S) in the supplemental material.

Atom	f^+				f^-				f^0			
	B3LYP	BHandHLYP	B3PW91	WB97XD	B3LYP	BHandHLYP	B3PW91	WB97XD	B3LYP	BHandHLYP	B3PW91	WB97XD
1C	0.030	0.033	0.030	0.032	0.031	0.016	0.032	0.021	0.031	0.025	0.031	0.027
2C	0.026	0.027	0.026	0.024	0.059	0.059	0.059	0.067	0.042	0.043	0.042	0.045
3H	0.024	0.024	0.024	0.021	0.034	0.036	0.034	0.038	0.029	0.030	0.029	0.029
4H	0.024	0.020	0.025	0.019	0.034	0.038	0.034	0.038	0.029	0.029	0.029	0.029
5C	0.043	0.022	0.043	0.022	0.074	0.125	0.074	0.115	0.059	0.074	0.058	0.068
6C	0.033	0.026	0.033	0.028	0.028	0.019	0.028	0.019	0.031	0.023	0.031	0.024
7H	0.037	0.024	0.037	0.029	0.027	0.021	0.027	0.022	0.032	0.022	0.032	0.026
8C	0.082	0.026	0.081	0.038	0.029	0.008	0.029	0.009	0.056	0.017	0.055	0.023
9C	0.144	0.232	0.144	0.209	0.015	0.010	0.015	0.012	0.080	0.121	0.079	0.110
10O	0.030	0.023	0.030	0.023	0.063	0.092	0.062	0.092	0.046	0.058	0.046	0.058
11O	0.055	0.036	0.056	0.036	0.232	0.458	0.232	0.406	0.144	0.247	0.144	0.221
12O	0.030	0.035	0.030	0.032	0.113	0.021	0.113	0.043	0.072	0.028	0.072	0.037
13H	0.020	0.023	0.020	0.024	0.034	0.012	0.034	0.019	0.027	0.017	0.027	0.021
14O	0.042	0.015	0.042	0.020	0.034	0.010	0.034	0.010	0.038	0.012	0.038	0.015
15H	0.028	0.016	0.027	0.019	0.020	0.009	0.020	0.010	0.024	0.013	0.023	0.014
16O	0.094	0.044	0.094	0.056	0.087	0.019	0.089	0.022	0.091	0.031	0.091	0.039
17O	0.073	0.106	0.073	0.099	0.023	0.010	0.023	0.013	0.048	0.058	0.048	0.056
18H	0.038	0.053	0.038	0.059	0.016	0.009	0.016	0.012	0.027	0.031	0.027	0.035
19O	0.145	0.215	0.146	0.211	0.047	0.027	0.047	0.033	0.096	0.121	0.096	0.122

Table 4. Condensed Fukui function values for nucleophilic attacks on GA at the X/6-311G (d,p) level of theory (where X = B3LYP,[40,41] B3PW91,[42] BHandHLYP,[43] and WB97XD[44]), in the aqueous phase employing Hirshfeld population and equations (6S-8S) in the supplemental material.

Atom	f^+				f^-				f^0			
	B3LYP	BHandHLYP	B3PW91	WB97XD	B3LYP	BHandHLYP	B3PW91	WB97XD	B3LYP	BHandHLYP	B3PW91	WB97XD
1C	0.027	0.031	0.027	0.029	0.032	0.041	0.032	0.027	0.029	0.036	0.030	0.028
2C	0.037	0.031	0.037	0.030	0.054	0.064	0.054	0.068	0.046	0.047	0.046	0.049
3H	0.036	0.027	0.036	0.026	0.032	0.037	0.032	0.037	0.034	0.032	0.034	0.031
4H	0.036	0.028	0.037	0.027	0.032	0.035	0.032	0.039	0.034	0.032	0.035	0.033
5C	0.096	0.032	0.099	0.042	0.061	0.051	0.060	0.103	0.078	0.042	0.080	0.073
6C	0.027	0.020	0.027	0.021	0.033	0.030	0.033	0.021	0.030	0.025	0.030	0.021
7H	0.032	0.025	0.031	0.024	0.030	0.025	0.030	0.023	0.031	0.025	0.030	0.023
8C	0.043	0.006	0.037	0.005	0.039	0.016	0.040	0.013	0.041	0.011	0.038	0.009
9C	0.128	0.234	0.129	0.216	0.010	0.009	0.010	0.006	0.069	0.122	0.070	0.111
10O	0.045	0.022	0.046	0.025	0.057	0.051	0.056	0.087	0.051	0.036	0.051	0.056
11O	0.105	0.050	0.109	0.060	0.182	0.143	0.180	0.352	0.144	0.097	0.145	0.206
12O	0.033	0.037	0.033	0.034	0.148	0.283	0.147	0.089	0.090	0.160	0.090	0.062
13H	0.020	0.023	0.019	0.027	0.041	0.069	0.041	0.030	0.030	0.046	0.030	0.028
14O	0.024	0.009	0.022	0.010	0.039	0.014	0.040	0.013	0.032	0.011	0.031	0.011
15H	0.018	0.013	0.017	0.014	0.024	0.015	0.024	0.012	0.021	0.014	0.021	0.013
16O	0.060	0.030	0.054	0.028	0.112	0.043	0.116	0.029	0.086	0.037	0.085	0.028
17O	0.062	0.105	0.064	0.099	0.017	0.019	0.017	0.010	0.040	0.062	0.040	0.054
18H	0.036	0.055	0.036	0.060	0.016	0.017	0.016	0.012	0.026	0.036	0.026	0.036
19O	0.135	0.222	0.138	0.224	0.040	0.038	0.040	0.029	0.088	0.130	0.089	0.126

If one plots the reduced density gradient vs. sign (λ_2), peaks with negative signs indicate binding interactions, whereas peaks with positive values indicate non-bonding interactions.[58]

It is important to note that the evaluation of non-covalent interactions is highly dependent on the selection of the basis set and the method used for electron correlation correction. In this context, literature suggests that the wB97XD functional is particularly well-suited for predicting properties associated with these types of interactions.[59,60] The intermolecular interactions of HA (Fig. 8a) and GA (Fig. 8b). Figure 8a reveals that the peak at –0.025 corresponds to a stabilizing interaction associated with the presence of intramolecular hydrogen bonds between the carboxyl and hydroxyl groups at C-3. The peaks at –0.015 and –0.010 are related to intermolecular hydrogen bonds between the carboxyl at C-3 and the hydrogen atoms in the oxolane structure, at -0.005 correspond to stabilizing interactions between the two carboxyl subtituents at C-2 and C-3. In the case of repulsive intermolecular interactions, the peak at 0.005 corresponds to repulsive oxygen-oxygen interactions, and the peak at 0.010 is related to repulsive interactions between the hydrogen atoms in the oxolane structure and the carboxyl group at C-2. The peaks at 0.025 and 0.045 are related to the interaction between the carboxyl at C-2 and the hydroxyl group at C-3 and repulsion within the oxolane. On the other hand, Figure 8b shows a peak at –0.025 corresponding to intramolecular hydrogen bonding between the carboxyl and hydroxyl groups at C-2. Peaks of –0.015 and –0.010 are associated with attractive interactions between the carboxyl at C-3 and the oxolane and between the carboxyl at C-2 and the hydroxyl at C-3. While for the repulsive interactions, peaks at 0.005, 0.010, and 0.015 were associated with the repulsion between the two carboxyl groups of the molecule at C-2 and C-3, the oxygen-oxygen repulsion between the carbonyl of the lactone and the carboxyl group at C-2, and between the carboxyl at C-3 and the lactone center, respectively. Finally, peaks 0.025 and 0.045 correspond to the repulsive interaction between the carboxyl at C-2 and the hydroxyl at C-3. According to these results, the diasteroisomer (2*S*,3*R*) is stabilized by an interaction identified at –0.005, while the diasteroisomer (2*S*,3*S*) is stabilized by the interaction recorded at 0.015, which suggests that HA is more stable than

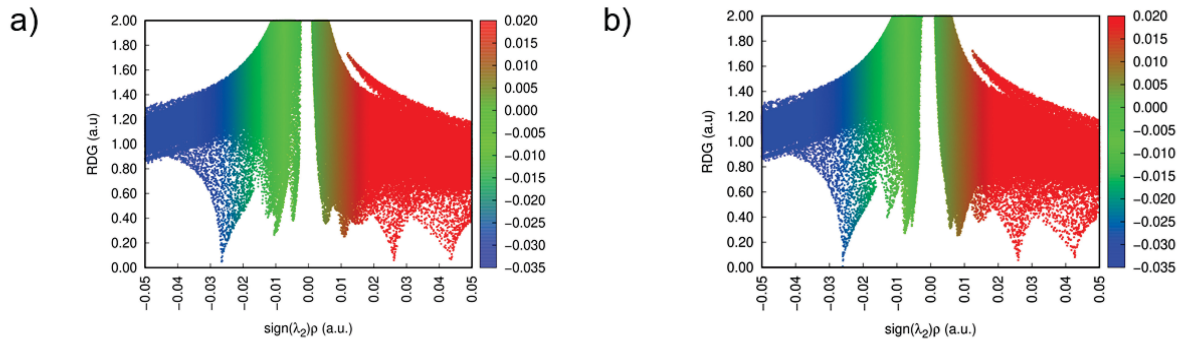

Figure 8. Plot of the reduced density gradient vs. sign(λ_2)ρ for a) hibiscus acid and b) garcinia acid in the aqueous phase.

GA. These results were verified with the molecular isosurfaces, $s(r)$, plotted for HA (Fig. 9a) and for GA (Fig. 9b), where the color code coincides in the peaks of the diagram and in the isosurface plot. In these plots, the red isosurfaces indicate a non-favorable interaction, and the green and blue isosufaces indicate favorable intermolecular interactions.

The second-order perturbation theory of the Fock matrix[52] was applied to estimate the donor-acceptor interactions in HA and GA. This type of analysis has proven successful in evaluating the stabilization energy and charge transfer in a molecular system.[61] For each donor (i) and acceptor (j), the stabilization energy $E(2)$, associated with the delocalization of electrons between i and j, was evaluated using the following equation:

$$E(2) = \Delta E_{ij} = q_i \frac{F(i,j)^2}{E_j - E_i} \quad (9)$$

where: q_i represents the occupancy of the donor orbital, while E_i and E_j are the orbital energy values of the donor and acceptor, respectively; the Fock matrix elements are denoted as; Table 5 presents the second-order perturbation energies $E(2)$ (in kcal mol^{-1}) corresponding to the most significant charge transfer interactions (donor ⟶ acceptor) in HA, obtained using the WB97XD/6-311++G(2d,2p) method. It is important to note that, in all cases, the donors are lone pairs (LP) of electrons on oxygen atoms (O17, O14, O10, O11, O16), where "LP" stands for "Lone Pair" referring to a pair of electrons not involved in bonding. Meanwhile, the electron acceptor is an empty orbital on a carbon atom (C) interacting with the lone pair of electrons on oxygen. For HA, the highest interaction energy ($E(2)$) is 70.34 kcal mol^{-1} between LP(2) O17 (the second lone pair on oxygen atom O17) and BD*(2) C9-O19 (an excited or antibonding bonding orbital, where "BD*" refers to "Bonding Molecular Orbital," representing the interaction of the lone pair with an empty or partially filled molecular orbital on carbon C9). However, the energy difference $E_i - E_j$ is not the largest in this case, as the highest difference is observed between LP(2) O16 and BD*(1) C8-O14 (0.79). On the other hand, the interaction strength appears to be relatively similar for all interactions, with values close to 0.17. Although the interaction between LP(2) O17 and BD*(2) C9-O19 is the most favorable, suggesting a favorable geometric arrangement in which the involved orbitals have good overlap, the energy difference ($E_i - E_j$) does not drastically affect the interaction strength. As both the interaction energy ($E(2)$) and energy difference $E_i - E_j$ decrease, the interaction strength remains relatively constant. This indicates that the energy difference does not significantly impact the interaction strength within this dataset. Similar results are observed for the GA molecule, as shown in Table 6, where the interaction between LP(2) O17 and BD*(2) C9-O19 is also the most favorable.

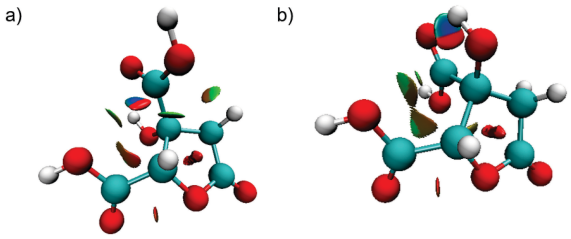

Figure 9. s (p = 0.2) isosurface of a) HA and b) GA in aqueous

Table 5. The second-order perturbation energies $E(2)$ (kcal mol^{-1}) corresponding to the most important charge transfer interactions (donor ⟶ acceptor) in HA evaluated at the using WB7XD/6-311G (d,p) level of theory.

Donor NBO (i)	Acceptor NBO (j)	$E(2)$ / kcal mol^{-1}	$E_i - E_j$ / a.u.	$F(i,j)$ /a.u.
LP(2) O17	BD*(2) C9- O19	70.34	0.49	0.167
LP(2) O14	BD*(2) C8- O16	64.92	0.50	0.162
LP(2) O10	BD*(2) C5- O11	60.57	0.49	0.154
LP(2) O11	BD*(1) C5- O10	46.39	0.77	0.171
LP(2) O16	BD*(1) C8- O14	43.85	0.79	0.168

Table 5. The second-order perturbation energies $E(2)$ (kcal mol^{-1}) corresponding to the most important charge transfer interactions (donor ⟶ acceptor) in GA evaluated at the using WB7XD/6-311G (d,p) level of theory.

Donor NBO (i)	Acceptor NBO (j)	$E(2)$ / kcal mol^{-1}	$E_i - E_j$ / a.u.	$F(i,j)$ / a.u.
LP(2) O17	BD*(2) C9- O19	70.63	0.49	0.167
LP(2) O14	BD*(2) C8- O16	65.26	0.50	0.162
LP(2) O10	BD*(2) C5- O11	60.37	0.49	0.154
LP(2) O11	BD*(1) C5- O10	46.47	0.77	0.171
LP(2) O16	BD*(1) C8- O14	43.86	0.78	0.168

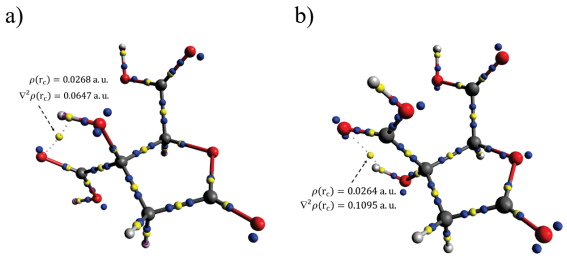

Figure 10. Molecular graphs of a) HA and b) GA. The small yellow and blue dots represent the bond critical points and lone pairs (LP), respectively.

Also, a topological analysis of HA and GA was performed using Bader's Atoms in Molecules (AIM) theory,[62] as shown in Figure 10. The bond critical points (BCPs) along these interactions were identified, and the electronic density and Laplacian values were evaluated. The main differences were observed at the critical points indicated in Figures 10a and 10b. Notably, both points exhibit very similar electronic densities, though the BCP in HA shows a slightly higher density. However, the Laplacian of the density in GA is higher (0.1095 a.u.) compared to HA (0.0647 a.u.), indicating that the electron distribution in GA changes more rapidly in the vicinity of the BCP. This suggests that the BCP in GA is more sensitive to variations in electronic density, which may account for the observed differences in local reactivity when compared to HA.

CONCLUSION

In the present work, the molecular chemical reactivity of the structures of HA and GA in the aqueous phase was studied. By calculating the local reactivity parameters, it was observed that both diasteroisomers have the same global reactivity. The results of the Fukui Function evaluation using the FD approach suggest that the distribution of active sites for HA, in the case of nucleophilic attacks, is located on the carboxyl at C-3; for electrophilic attacks, the more active sites were the oxygen atom of the carbonyl group of the carboxyl at C-2, the oxygen atom in the oxolane, and the hydroxyl group at C-3; and for free radical attacks, the more reactive positions are on the carboxyl groups at C-2 and C-3 and the oxygen atom in the oxolane. For GA, the more susceptible sites to nucleophilic attack are the carboxyl group at C-3, in addition to the oxygen in the oxolane. When electrophilic attacks occur, they are the oxygen atoms of the carbonyl group in the carboxyl group at C-2, the oxygen in the oxolane, and the hydroxyl group at C-3. For free radical attacks focus on the carboxyl groups at C-2 and C-3 and on the oxygen at oxolane. NBO results were used to assess donor-acceptor interactions in HA and GA. The results show that the most favorable interaction is between LP(2) O17 and BD*(2) C9-O19. Analysis of bond critical points reveals a higher Laplacian of density in GA compared to HA, indicating that the BCP in GA is more sensitive to changes in electronic density, which may explain the differences in reactivity between these compounds.

Acknowledgment. WLO acknowledges CONACYT for the scholarship granted for Doctoral studies. L. H. M. H. thankfully acknowledges the computer resources, technical expertise, and support provided by the Laboratorio Nacional de Supercómputo del Sureste de México, a CONACYT member of the network of National laboratories through project No. 202501011N. The authors thank to Universidad Autónoma del Estado de Hidalgo for the funding granted for this work through Project PAO-2022-1389 UAEH. LHMH, GAAR and MSZ acknowledge to the SNI for the distinction of his membership and the stipend received. Guanajuato National Laboratory (CONACyT 123732) is acknowledged for supercomputing resources.

Supplementary Information. Supporting information to the paper is attached to the electronic version of the article at: http://doi.org/10.5562/cca4153.

PDF files with attached documents are best viewed with Adobe Acrobat Reader which is free and can be downloaded from Adobe's web site.

REFERENCES

[1] P. Chandrasekaran, R. Weiskirchen, *Int. J. Mol. Sci.* **2024**, *25*, 1882. https://doi.org/10.3390/ijms25031882

[2] R. Ruze, T. Liu, X. Zou, J. Song, Y. Chen, R. Xu, X. Yin, Q. Xu, *Front. Endocrinol. (Lausanne)* **2023**, *14*, 1–23. https://doi.org/10.3389/fendo.2023.1161521

[3] K. A. Naser, A. Gruber, G. A. Thomson, *Int. J. Clin. Pract.* **2006**, *60*, 1093–1097. https://doi.org/10.1111/j.1742-1241.2006.01003.x

[4] L. O. Chuah, W. Y. Ho, B. K. Beh, S. K. Yeap, *Evidence-based Complement. Altern. Med.* **2013**, *2013*, 1–17. https://doi.org/10.1155/2013/751658
[5] R. J. Rodgers, M. H. Tschöp, J. P. H. Wilding, *Dis. Model. Mech.* **2012**, *5*, 621. https://doi.org/10.1242/dmm.009621
[6] M. A. Nauck, D. R. Quast, J. Wefers, J. J. Meier, *Mol. Metab.* **2021**, *46*, 101102. https://doi.org/10.1016/j.molmet.2020.101102
[7] I. S. Padda, A. U. Mahtani, M. Parmar, in *StatPearls*, StatPearls Publishing **2023**.
[8] W. A. Aldhaleei, T. M. Abegaz, A. S. Bhagavathula, *Pharm.* **2024**, *17*, 199. https://doi.org/10.3390/ph17020199
[9] A. Tentolouris, P. Vlachakis, E. Tzeravini, I. Eleftheriadou, N. Tentolouris, *Int. J. Environ. Res. Public Health* **2019**, *16*, 2965. https://doi.org/10.3390/ijerph16162965
[10] H. Y. Aati, A. Ismail, M. E. Rateb, A. M. AboulMagd, H. M. Hassan, M. H. Hetta, *Plants* **2022**, *11*, 2521. https://doi.org/10.3390/plants11192521
[11] A. N. M. Ansori, V. D. Kharisma, A. A. Parikesit, F. A. Dian, R. T. Probojati, M. Rebezov, P. Scherbakov, P. Burkov, G. Zhdanova, A. Mikhalev, et al., *Pharmacogn. J.* **2022**, *14*, 85–90. https://doi.org/10.31602/al-adl.v14i2.6582
[12] V. D. Kharisma, A. N. M. Ansori, Y. Antonius, I. Rosadi, A. A. A. Murtadlo, V. Jakhmola, M. Rebezov, N. Maksimiuk, E. Kolesnik, P. Burkov, et al., *J. Pharm. Pharmacogn. Res.* **2023**, *11*, 743–756. https://doi.org/10.56499/jppres23.1650_11.5.743
[13] D. Muralitharan, V. Varadharajan, B. Venkidasamy, *J. Mol. Recognit.* **2023**, *36*, e3055. https://doi.org/10.1002/jmr.3055
[14] E. Akbaba, D. Karatas, *Iğdır Üniversitesi Fen Bilim. Enstitüsü Derg.* **2023**, *13*, 872–888. https://doi.org/10.21597/jist.1187616
[15] C. Parga-Lozano, *Duazary* **2020**, *17*, 1–3. https://doi.org/10.21676/2389783X.3597
[16] E. Shawky, A. A. Nada, R. S. Ibrahim, *RSC Adv.* **2020**, *10*, 27961–27983. https://doi.org/10.1039/D0RA05126H
[17] P. L. Polavarapu, E. A. Donahue, G. Shanmugam, G. Scalmani, E. K. Hawkins, C. Rizzo, I. Ibnusaud, G. Thomas, D. Habel, D. Sebastian, et al., *J. Phys. Chem. A* **2011**, *115*, 5665–5673. https://doi.org/10.1021/jp202501y
[18] M. H. Baky, H. Fahmy, M. A. Farag, *ACS Omega* **2022**, *7*, 25948–25957. https://doi.org/10.1021/acsomega.2c02838
[19] A. Gogoi, N. Gogoi, B. Neog, *Int. J. Pharm. Sci. Res.* **2014**, *5*, 4995–4999.
[20] B. S. Jena, G. K. Jayaprakasha, R. P. Singh, K. K. Sakariah, *J. Agric. Food Chem.* **2001**, *50*, 10–22. https://doi.org/10.1021/jf010753k
[21] T. Yamada, H. Hida, Y. Yamada, *Appl. Microbiol. Biotechnol.* **2007**, *75*, 977–982. https://doi.org/10.1007/s00253-007-0962-4
[22] H. Hida, T. Yamada, Y. Yamada, *Biosci. Biotechnol. Biochem.* **2005**, *69*, 1555–1561. https://doi.org/10.1271/bbb.69.1555
[23] M. Tomar, R. P. Rao, P. Dorairaj, A. Koshta, S. Suresh, M. Rafiq, R. Kumawat, R. Paramesh, U. V. Babu, K. V. Venkatesh, *RSC Adv.* **2019**, *9*, 18578–18588. https://doi.org/10.1039/C9RA01345H
[24] D. Jamrozik, W. Borymska, I. Kaczmarczyk-Żebrowska, *Foods* **2022**, *11*. https://doi.org/10.3390/foods11142134
[25] S. Zulfiqar, L. J. Marshall, C. Boesch, *Hum. Nutr. Metab.* **2022**, *30*, 200164. https://doi.org/10.1016/j.hnm.2022.200164
[26] O. A. Olajide, V. U. Iwuanyanwu, I. Lepiarz-Raba, A. A. Al-Hindawi, M. A. Aderogba, H. L. Sharp, R. J. Nash, *Phyther. Res.* **2021**, *35*, 6963–6973. https://doi.org/10.1002/ptr.7315
[27] J. B. Radke, J. M. Kingery, J. Maakestad, M. D. Krasowski, *Toxicol. Reports* **2019**, *6*, 1040–1046. https://doi.org/10.1016/j.toxrep.2019.10.006
[28] Y. Takeda, Y. Okuyama, H. Nakano, Y. Yaoita, K. Machida, H. Ogawa, K. Imai, *Food Environ. Virol.* **2020**, *12*, 9–19. https://doi.org/10.1007/s12560-019-09408-x
[29] B. L. S. do Espirito Santo, L. F. Santana, W. H. Kato Junior, F. de O. de Araújo, D. Bogo, K. de C. Freitas, R. de C. A. Guimarães, P. A. Hiane, A. Pott, W. F. de O. Filiú, *Molecules* **2020**, *25*, 4513. https://doi.org/10.3390/MOLECULES25194513
[30] C. Suhandi, S. S. Alfathonah, A. N. Hasanah, *Molecules* **2023**, *28*, 5187. https://doi.org/10.3390/molecules28135187
[31] W. Sun, M. H. Shahrajabian, Q. Cheng, *Appl. Sci.* **2021**, *11*, 7889. https://doi.org/10.3390/APP11177889
[32] A. Thomas, M. Prajila, K. M. Shainy, A. Joseph, *J. Mol. Liq.* **2020**, *312*, 113369. https://doi.org/10.1016/j.molliq.2020.113369
[33] I. Ibnusaud, P. T. Thomas, R. N. Rani, P. V. Sasi, T. Beena, A. Hisham, *Tetrahedron* **2002**, *58*, 4887–4892. https://doi.org/10.1016/S0040-4020(02)00431-3
[34] R. G. Parr, W. Yang, *Density-Functional Theory of Atoms and Molecules*, First ed., Oxford University Press, New York **1989**.
[35] R. Pal, P. K. Chattaraj, *J. Indian Chem. Soc.* **2021**, *98*, 100008. https://doi.org/10.1016/j.jics.2021.100008

[36] R. G. Parr, L. V. Szentpály, S. Liu, *J. Am. Chem. Soc.* **1999**, *121*, 1922–1924. https://doi.org/10.1021/ja983494x
[37] R. G. Parr, W. Yang, *J. Am. Chem. Soc.* **1984**, *106*, 4049–4050. https://doi.org/10.1021/ja00326a036
[38] W. Yang, W. J. Mortier, *J. Am. Chem. Soc.* **1986**, *108*, 5708–5711. https://doi.org/10.1021/ja00279a008
[39] R. Krishnan, J. S. Binkley, R. Seeger, J. A. Pople, *J. Chem. Phys.* **1980**, *72*, 650–654. https://doi.org/10.1063/1.438955
[40] K. Raghavachari, *Theor. Chem. Accounts* **2000**, *103*, 361–363. https://doi.org/10.1007/s002149900065
[41] A. D. Becke, *Phys. Rev. A.* **1988**, *38*, 3098–3100. https://doi.org/10.1103/PhysRevA.38.3098
[42] A. D. Becke, *J. Chem. Phys.* **1993**, *98*, 5648–5652. https://doi.org/10.1063/1.464913
[43] A. D. Becke, *J. Chem. Phys.* **1993**, *98*, 1372–1377. https://doi.org/10.1063/1.464304
[44] J. Da Chai, M. Head-Gordon, *Phys. Chem. Chem. Phys.* **2008**, *10*, 6615–6620. https://doi.org/10.1039/b810189b
[45] S. Miertuš, E. Scrocco, J. Tomasi, *Chem. Phys.* **1981**, *55*, 117–129. https://doi.org/10.1016/0301-0104(81)85090-2
[46] S. Miertuš, J. Tomasi, *Chem. Phys.* **1982**, *65*, 239–245. https://doi.org/10.1016/0301-0104(82)85072-6
[47] M. J. Frisch, G. W. Trucks, H. B. Schlegel, G. E. Scuseria, M. A. Robb, J. R. Cheeseman, G. Scalmani, V. Barone, G. A. Petersson, H. Nakatsuji, X. Li, M. Caricato, A. Marenich, J. Bloino, B. G. Janesko, R. Gomperts, B. Mennucci, H. P. Hratchian, J. V. Ortiz, A. F. Izmaylov, J. L. Sonnenberg, D. Williams-Young, F. Ding, F. Lipparini, F. Egidi, J. Goings, B. Peng, A. Petrone, T. Henderson, D. Ranasinghe, V. G. Zakrzewski, J. Gao, N. Rega, G. Zheng, W. Liang, M. Hada, M. Ehara, K. Toyota, R. Fukuda, J. Hasegawa, M. Ishida, T. Nakajima, Y. Honda, O. Kitao, H. Nakai, T. Vreven, K. Throssell, J. A. Montgomery, Jr., J. E. Peralta, F. Ogliaro, M. Bearpark, J. J. Heyd, E. Brothers, K. N. Kudin, V. N. Staroverov, T. Keith, R. Kobayashi, J. Normand, K. Raghavachari, A. Rendell, J. C. Burant, S. S. Iyengar, J. Tomasi, M. Cossi, J. M. Millam, M. Klene, C. Adamo, R. Cammi, J. W. Ochterski, R. L. Martin, K. Morokuma, O. Farkas, J. B. Foresman, and D. J. Fox, *Gaussian 09, Revision A.02*, Gaussian, Inc., Wallingford CT, **2016**.
[48] J. M. Dennington, R. D. Keith, T. A. Millam, *GaussView, Version 5.0.8*, Semichem Inc., Shawnee Mission KS, **2009**.
[49] M. Thompson, *ACS Meet.*, Philadelphia, **2004**.
[50] A. Allouche, *J. Comput. Chem.* **2012**, *32*, 174–182. https://doi.org/10.1002/jcc.21600
[51] T. Lu, F. Chen, *J. Comput. Chem.* **2012**, *33*, 580–592. https://doi.org/10.1002/jcc.22885
[52] E. D. Glendening et al., NBO Version 3.1, **1998**.
[53] L. A. Portillo-Torres et al., *Antibiot.* **2019**, *8*, 218.
[54] J. P. Merrick, D. Moran, L. Radom, *J. Phys. Chem. A.* **2007**, *111*, 11683–11700. https://doi.org/10.1021/jp073974n
[55] J. L. Gázquez, *J. Phys. Chem. A.* **1997**, *101*, 4591–4593. https://doi.org/10.1021/jp970643+
[56] F. L. Hirshfeld, *Theor. Chim. Acta.* **1977**, *44*, 129–138. https://doi.org/10.1007/BF00549096
[57] P. K. Chattaraj, *Chemical Reactivity Theory: A Density Functional View*, CRC Press/Taylor & Francis **2009**. https://doi.org/10.1201/9781420065442
[58] E. R. Johnson, S. Keinan, P. Mori-Sánchez, J. Contreras-García, A. J. Cohen, W. Yang, *J. Am. Chem. Soc.* **2010**, *132*, 6498–6506. https://doi.org/10.1021/ja100936w
[59] L. H. Mendoza-Huizar, E. G. Sánchez, L. O. Solís Sánchez, *Croat. Chem. Acta.* **2023**, *96*, 125–131. https://doi.org/10.5562/cca4009
[60] T. Karthick, P. Tandon, K. Srivastava, S. Singh, *Arab. J. Chem.* **2018**, *11*, 591–608. https://doi.org/10.1016/j.arabjc.2017.10.012
[61] C. Karthika, R. Praveena, S. Ramachandran, K. Sadasivam, G. Salgado, P. Muñoz, L. Gerli, L. H. Mendoza-Huizar, *Croat. Chem. Acta.* **2020**, *93*, 147–155. https://doi.org/10.5562/cca3695
[62] R. F. W. Bader, *Atoms in Molecules: A Quantum Theory*, Oxford University Press, **1990**.